

1 Homomorphic ZW Chromosomes in a Wild Strawberry Show
2 Distinctive Recombination Heterogeneity but a Small Sex-Determining
3 Region

4

5 Jacob A Tennessen¹, Rajanikanth Govindarajulu^{2,3}, Aaron Liston⁴ and Tia-Lynn Ashman^{2*}

6

7 ¹Department of Integrative Biology, Oregon State University, Corvallis, OR, USA

8 ²Department of Biological Sciences, University of Pittsburgh, Pittsburgh, PA, USA

9 ³Current affiliation: Department of Biology, West Virginia University, Morgantown, WV, USA

10 ⁴Department of Botany and Plant Pathology, Oregon State University, Corvallis, OR, USA

11 *Author for Correspondence: Tia-Lynn Ashman, Department of Biological Sciences, University
12 of Pittsburgh, 215 Clapp Hall, 4249 Fifth Avenue, Pittsburgh, PA 15260, Phone: (412) 624-
13 0984, Fax: (412) 624-4759, tial@pitt.edu

14 Short title: Strawberry Sex Chromosome Recombination Patterns

15

16 **Abstract**

17 Sex chromosomes play a prominent role in development and evolution and have several
18 characteristic features that distinguish them from autosomes. Across diverse taxa, recombination
19 is typically suppressed at the sex-determining region (SDR) and proportionally elevated in the
20 remainder of the chromosome or pseudoautosomal region (PAR). However, in most model taxa
21 the sex chromosomes are ancient and highly differentiated from autosomes, and thus little is
22 known about recombination dynamics of homomorphic sex chromosomes with incipient sex-
23 determining mechanisms. Here we examine male function (pollen production) and female
24 function (fruit production) in crosses of the dioecious octoploid strawberry *Fragaria chiloensis*
25 in order to map the small and recently evolved SDR controlling both traits and to examine
26 recombination patterns on the young ZW chromosome. The SDR occurs in a narrow 280kb
27 window, in which the maternal recombination rate is lower than in the orthologous paternal
28 region and the genome-wide average rate, but within the range of autosomal rate variation. In
29 contrast to the SDR, the ZW recombination rate in the PAR is much higher than the rates of the
30 ZZ or autosomal linkage groups, substantially overcompensating for the SDR rate. By
31 extensively sequencing sections of the SDR vicinity in several crosses and unrelated plants, we
32 show that W-specific divergence is elevated within a portion of the SDR and find only a single
33 SNP to be in high linkage disequilibrium with sex, suggesting that any W-specific haplotype
34 protected from recombination is not large. We hypothesize that selection for recombination
35 suppression within the small SDR may be weak, but that fluctuating sex ratios could favor
36 elevated recombination in the PAR to remove deleterious mutation on the W. Thus these results
37 illuminate the recombination dynamics of a nascent sex chromosome with a modestly diverged
38 SDR, which could be typical of other dioecious plants.

39

40 **Author Summary**

41 In many species, the sex-determining chromosomes have distinct features relative to the
42 rest of the genome, including unusual recombination rates. The wild strawberry *Fragaria*
43 *chiloensis* possesses a recently evolved sex chromosome that illuminates the early stages of sex
44 chromosome differentiation and adjustment of recombination rates. We examined the
45 phenotypes of both male function (pollen production) and female function (fruit production)
46 among hundreds of strawberry offspring resulting from several crosses, which allowed us to
47 identify a narrow chromosomal region influencing both of these traits. We then examined and
48 compared maternal and paternal recombination rates in the vicinity of this sex-determining
49 region and all along the ZW sex chromosome. A region of suppressed recombination
50 surrounding the sex gene(s) is relatively small, but substantial differences in recombination rate
51 among the parents are seen on the sex chromosome outside of this region. These results help us
52 to understand how sex-determining regions appear, are maintained, and impact the rest of the
53 genome.

54

55 **Introduction**

56 Sex chromosomes are genomic oddities, often with distinctive inheritance patterns,
57 effective population sizes, recombination frequencies, and structural arrangements, leading to
58 unique evolutionary dynamics [1],[2]. These unusual features give sex chromosomes a key role
59 in numerous biological phenomena such as speciation [3-5], disease progression [6], whole-
60 genome duplications [7],[8], and contribution to the genetics of complex traits including sexual

61 dimorphism [9-12]. Sex determination mechanisms across the tree of life are diverse, and include
62 male heterogamety (XY inheritance), female heterogamety (ZW inheritance), and more complex
63 scenarios (reviewed in [13]). Although sex phenotype is typically determined by only one or two
64 genes, these functional element(s) frequently reside within a larger sex-determining region
65 (SDR) which is inherited as a unit. The remainder of the sex chromosome outside the SDR,
66 known as the pseudo-autosomal region (PAR), can also have distinct properties that distinguish it
67 from ordinary autosomal sequence [14],[15]. One of the defining features of sex chromosomes is
68 a specific and repeatable pattern of heterogeneity in recombination rate that has been seen across
69 diverse taxa including vertebrates, arthropods, fungi, and flowering plants [16],[17]. That is, the
70 SDR typically shows suppressed recombination in the heterogametic parent, while the PAR may
71 show elevated recombination in these same individuals (reviewed in [15],[18]). The adaptive
72 basis for these recombination patterns has been extensively examined theoretically [13],[19]. In
73 brief, if an SDR-linked locus harbors an allele that is advantageous in one sex and
74 disadvantageous in the other (i.e. sexually antagonistic mutations), recombinants will have
75 decreased fitness and recombination suppression will be favored. In the case where sex is
76 determined by two loci both carrying fertility/sterility mutations, recombinants lack both male
77 and female fertility alleles and are thus neuters, making the suppression of recombination highly
78 advantageous [1],[19],[20]. As recombination is suppressed, differential substitutions and
79 transposable elements accumulate within the widening SDR, resulting in evolutionary strata of
80 sequence divergence between X/Z and Y/W [16],[21]. Recombination is nonetheless usually
81 required for faithful chromosome segregation, so the recombination rate of the PAR may
82 increase in the heterogametic sex to compensate for the SDR [15],[17]. Even with elevated PAR

83 recombination, the total sex chromosome recombination rate averaged across the PAR and SDR
84 is usually less than or equal to the genome-wide average [15].

85 The most extensively studied sex chromosomes, primarily in model animals systems, are
86 ancient and highly heteromorphic, making it difficult to understand the initial stages of sex
87 chromosome evolution [22],[23]. However, a much greater diversity of sex determining systems
88 exists, especially in plants [13],[18],[24]. While few of the 15,600 dioecious species of flowering
89 plants [25] have heteromorphic sex chromosomes, and the genetics of sex determination in the
90 vast majority are unknown [2],[26], several recent studies have revealed homomorphic sex
91 chromosomes with small SDRs [20],[27-34]. For instance, strikingly small SDR were identified
92 in *Vitis* and *Populus*. The *Vitis* sex locus has been mapped to 143kb, so if there is a suppressed-
93 recombination SDR at all, it must occur within this window [28]. The SDR in *Populus* is only
94 ~100kb yet determines both male and female function [32]. The slightly larger SDRs (1-10Mb)
95 in plant taxa such as *Actinidia* [34], *Carica* [29], and *Asparagus* (A. Harkess personal
96 communication) are still relatively small on a chromosomal scale, and vastly so relative to
97 cytogenetically heteromorphic chromosomes. Most previous studies in plants have examined XY
98 systems in diploids (but see [33]), leaving open the question of whether similar small SDRs are
99 common in ZW systems or in polyploids, the latter of which gains special importance in
100 flowering plants given the potential association between dioecy and polyploidy [8],[35].
101 Furthermore, homomorphic sex chromosomes may not necessarily display any recombination
102 heterogeneity, or it may be weak, and thus the resultant patterns of sequence divergence and
103 linkage disequilibrium may be subtle or nonexistent. Such chromosomes, which largely resemble
104 autosomes but for the SDR, could represent the precursors of heteromorphic chromosomes,
105 although these are rare in flowering plants [26]. Alternatively, SDRs may remain small for tens

106 of millions of years, as in ratite birds [36], or control of sex may turn over so rapidly among
107 distinct genomic regions that SDRs undergo minimal evolutionary change, as in the
108 homomorphic sex chromosomes of many frogs [7],[37]. The strength of selection for expansion
109 and divergence of the SDR likely depends on the degree of sexual dimorphism, and therefore the
110 number of genes with alleles showing sex-specific fitness [38]. Whatever their eventual fate,
111 homomorphic sex chromosomes, for which recombination still occurs along most or all of their
112 length, present several advantages for research: fine-mapping candidate causal sex genes,
113 assessing patterns of recombination heterogeneity, estimating the fitness of recombinants, and
114 inferring chromosomal evolution in response to sex linkage [11],[39].

115 The wild strawberries, genus *Fragaria*, are a model system for early sex chromosome
116 evolution [20],[40],[41]. Evolving from a hermaphroditic ancestor just 2 mya [42], the genus has
117 diversified into species displaying various sexual systems, including gynodioecy (females and
118 hermaphrodites), subdioecy (females, males, and hermaphrodites), and dioecy (females and
119 males). In the gynodioecious diploid *F. vesca* subsp. *bracteata*, at least two unlinked loci harbor
120 male sterility alleles, only one of which, on chromosome IV (out of seven haploid chromosomes,
121 designated with Roman numerals I-VII), is heterozygous in females [43],[44]. *Fragaria vesca*
122 subsp. *bracteata* is an ancestor of allo-octoploid *Fragaria* species ($2n=8x=56$), having provided
123 the chloroplast genome, a putative mitochondrial cytoplasmic male sterility (CMS) gene, and one
124 of the four nuclear subgenomes (subgenome Av out of Av, B1, B2, and Bi) [42],[45-47]. It does
125 not share its sex loci with the octoploid clade, though. Wild octoploid *F. virginiana* subsp.
126 *virginiana* possesses a female-heterozygous SDR at the start of linkage group VI-B2-m (i.e.,
127 haploid chromosome six, subgenome B2, maternal chromosome), while wild octoploid *F.*
128 *chiloensis* possesses a female-heterozygous SDR at the end of linkage group VI-Av-m

129 [11],[27],[45],[48]. Octoploid *Fragaria* are highly diploidized, such that these subgenomes
130 remain evolutionarily distinct [45]. Thus, sex determination in this genus has frequently evolved
131 independently, and/or exhibits a rapidly shifting genomic position. Moreover, since the octoploid
132 clade arose 1 mya [42], and SDRs are not shared among the dimorphic species they appear to be
133 some of the youngest studied to date.

134 *Fragaria chiloensis* occurs on or near the Pacific coasts of North and South America and
135 is divided into several subspecies. While *F. virginiana* is subdioecious [48], *F. chiloensis* is
136 nearly completely dioecious, although some hermaphrodites do occur [49]. Thus, *F. chiloensis*
137 has undergone perhaps the greatest sexual differentiation in the genus with respect to the
138 hermaphroditic *Fragaria* ancestor [40],[50]. Because male and female function both map to a
139 single maternal genomic location with no previously observed recombination between them [27],
140 *F. chiloensis* has all the hallmarks of a complete, albeit incipient, ZW sex chromosome. In fact,
141 as all other flowering plant sex chromosomes showing evidence of recent origin (homomorphic,
142 taxonomically restricted, small SDRs, etc.) are XY, *F. chiloensis* appears to possess the youngest
143 plant ZW chromosome yet characterized. However, neither the precise genomic location of the
144 SDR, its physical size, nor the recombination profile of the SDR-carrying chromosomes could be
145 determined from the initial SSR-based linkage map [27].

146 Here we characterize the *F. chiloensis* sex chromosome with respect to Z- or W-specific
147 recombination rates in the PAR and SDR, as well as recombination-dependent metrics like
148 sequence divergence and linkage disequilibrium. To achieve this goal, we first precisely define
149 the SDR by fine-mapping both male and female function. We substantially increase the numbers
150 of both molecular markers and progeny for a previously described cross [27] and also examine

151 the two other crosses and several additional unrelated individuals. By analyzing SNPs both
152 extremely close to the causal sex gene(s) and all along the sex chromosome, and by leveraging
153 the large and highly duplicated genome as an internal control for recombination estimates of
154 autosomes (i.e. of the autosomal VI homeologs and across the rest of the genome), we can infer
155 the initial evolutionary adjustments in recombination rate and divergence that occur in response
156 to sex linkage.

157

158 **Results**

159 **Phenotypes**

160 In order to define the SDR, we first phenotyped male and female function in hundreds of
161 plants. In our largest cross, HM×SAL [27], 1285 seeds germinated overall and we obtained
162 genotype and/or phenotype data from 1277 of these (S1 Table). We determined male function for
163 693 progeny (352 male sterile, 341 male fertile), and female function for 619 progeny (157 with
164 fruit set <5% and thus “female sterile” as defined in Goldberg et al. [27]; mean flower number =
165 15.5). Male and female function were highly negatively correlated ($R^2 = 0.75$; $p < 10^{-15}$), such
166 that 98% of male-sterile plants showed at least 5% fruit set, while only 50% of male-fertile
167 plants showed at least 5% fruit set (Fig 1). Including total flower number in multiple regression
168 analysis did not significantly improve the proportion of variance explained in the simple linear
169 regression, suggesting little contribution of plant size to the relation between male and female
170 function ($R^2 = 0.76$; $p < 10^{-6}$). Similar phenotype distributions were observed among two sets of

171 20 offspring from independent crosses (EUR and PTR, S2 Table), and among 16 additional
172 unrelated plants (S3 Table).

173

174 **Fig 1. Sex phenotype distributions among HM×SAL offspring.** Male function is defined as the ability (male
175 fertility, blue) or inability (male sterility, pink) to produce mature pollen and is a binary trait found in approximately
176 half of the progeny. Female fertility is defined as the proportion of flowers producing fruit, and has a continuous
177 though bimodal distribution, shown here partitioned into bins of 5%. Male and female function are highly negatively
178 correlated, with nearly all male-fertile offspring showing <50% female fertility, and nearly all male-sterile offspring
179 showing >50% female fertility.

180

181 **Target capture mapping**

182 In order to initially map the SDR, we examined 42 HM×SAL offspring in a previously
183 described target capture dataset (S4 Table) [45]. We observed 23 male-fertile offspring and 19
184 male-sterile offspring. Male function mapped to the end of the VI-Av-m (maternal) linkage
185 group, as expected (LOD = 10.6; Fig 2) [27]. Specifically, the last recombination event before
186 the male function region occurs after reference genome position Fvb6_37.391Mb, after which
187 only a single male-sterile individual (which does not recombine anywhere on the linkage group)
188 has a genotype mismatching sex ($R^2 = 0.91$; $p < 10^{-15}$). Thus, these results suggest the SDR
189 occurs somewhere within the remaining 1.482Mb of the chromosome (the “SDR vicinity”), on
190 which we observed 10 SNPs in 9 targeted regions. An alternate, much weaker potential
191 quantitative trait locus (“QTL”) on linkage group II-Av-p (LOD = 3.6; Fig 2) was assumed to be
192 a statistical artifact and not pursued further, because it showed no significant association after

193 accounting for the QTL on VI-Av-m ($R^2 = 0.04$; $p > 0.1$). Female function showed the same
194 bimodal distribution as seen in the complete dataset (Fig 1), with most (59%) samples showing a
195 fruit set of either 0 (26%) or 1 (33%). The highest QTL for female function ($R^2 = 0.77$; $p < 10^{-13}$),
196 treated as a quantitative trait, occurred at the same location on VI-Av-m as male function,
197 peaking at Fvb6_37.391Mb (LOD = 18.8). The best two-QTL model for female function
198 included this region and was not significantly better than the single-QTL model.

199

200 **Fig 2. Male function LOD scores across the target capture linkage map.** The haploid chromosomes of the Fvb
201 reference genome are denoted by white rectangles along the x-axis. Each haploid chromosome occurs on each of
202 four subgenomes (Av, B1, B2, or Bi), shown as red or blue shaded bars. LOD scores for maternal and paternal
203 linkage maps are shown on the y-axis. The highest LOD score occurs on linkage group VI-Av-m, peaking at 10.6
204 for the last ten segregating sites in the linkage group, all aligning after Fvb6_37.391Mb. We subsequently validated
205 this region on VI-Av-m using hundreds of additional offspring, and thus the second-highest LOD peak on linkage
206 group II-Av-p (LOD = 3.6) appears not to be biologically meaningful.

207

208 **Amplicon fine mapping**

209 In order to further fine-map the SDR and calculate recombination rates, we genotyped
210 HM×SAL progeny at amplicons in the SDR vicinity. Of the 1285 HM×SAL progeny, we
211 obtained useable genotypes from 1235 offspring, including 1215 with Av-m genotypes and 1196
212 with Av-p genotypes (S1 Table). Although the set of useable sites varied slightly among each of
213 three sequencing rounds, by the third round we could genotype 36 segregating sites among 24
214 amplicons on VI-Av-m, and 24 segregating sites among 16 amplicons on VI-Av-p.

215 Recombinants were observed in all growing years and all sequencing rounds. We observed 32
216 plants that recombined on VI-Av-m, and these allowed us to further fine-map the male function
217 region to a 280kb section between Fvb_37.428Mb and Fvb6_37.708Mb (Fig 3). Specifically, we
218 observed near-perfect matches to male function at all sites between Fvb6_37.566Mb and
219 Fvb6_37.682Mb, with two male-fertile downstream recombinants showing mismatched
220 genotypes starting at Fvb6_37.708Mb, and two upstream recombinants at Fvb_37.428Mb, one of
221 which was phenotyped as male fertile. Seven individuals (one male-sterile from the target
222 capture genotyping described above, two more male-sterile, plus four male-fertile) had
223 genotypes mismatching male function in this region. These individuals did not recombine
224 anywhere in the SDR vicinity. With <1% of offspring mismatching, the correlation between
225 genotype in this male function region and male function phenotype was very strong ($R^2 = 0.96$; p
226 $< 10^{-15}$). The male function region resides entirely within a single scaffold of the Fvb reference
227 genome, scf0513124_6, minimizing the possibility of genome assembly errors in this region. The
228 original *F. vesca* genome annotation identified 68 genes in this male function region (S5 Table).
229 Two additional genes that do not overlap these genes appear in the most recent annotation [51]
230 (S5 Table).

231

232 **Fig 3. Fine-mapped male and female function and recombination rates across the SDR vicinity.** Physical
233 distance (Mb) along the distal end of Fvb6, encompassing portions of two genomic scaffolds (scf0513124_6 and
234 scf0513112a), is shown on the x-axis. All amplicon markers in the SDR vicinity in VI-Av-m (pink) and VI-Av-p
235 (light blue) are plotted, with relative linkage map position (cM, arbitrarily starting at 0) shown on the y-axis. An X
236 marks the position of the “universal marker” SNP on VI-Av-m which shows a high correlation with sex across the
237 full set of unrelated plants. Recombination rates can be inferred from the slopes of lines connecting VI-Av-m (pink)

238 and VI-Av-p (light blue) markers. Three colored bars with arbitrary vertical position indicate different estimates of
239 the SDR. The female-function region showing significantly higher correlation with fruit set than the surrounding
240 regions is indicated with a dark purple bar. The male-function region, bounded by the recombinants which decrease
241 the correlation with male function, is indicated with a dark red bar. The high *W* divergence region, within which
242 most *W*-specific SNPs are observed, is indicated by an orange bar. The SDR encompasses a relatively small portion
243 of the 39Mb chromosome. Maternal and paternal recombination rates are similar, except near the SDR, where they
244 are lower in the mother.

245
246 The highest LOD (145.9) to quantitative female function was observed on VI-Av-m at
247 Fvb6_37.428Mb, and correlations that were not significantly weaker than this were observed
248 between Fvb6_37.428-37.708Mb (LOD = 143.1-145.9), precisely the extent of the male function
249 region. Significantly worse correlations were observed upstream at Fvb6_37.391Mb (LOD =
250 142.4) and downstream at Fvb6_37.858Mb (LOD = 126.8), thus defining the limits of the 467kb
251 female function region (Fig 3). A QTL analysis that included the seven linkage groups in
252 homeologous group VI for which we had segregating markers among the sequenced amplicons
253 of the SDR vicinity (VI-B2-m not observed) supported the single QTL on VI-Av-m. The
254 correlation between SDR genotype and quantitative female function ($R^2 = 0.76$; $p < 10^{-15}$) was
255 similar to the correlation between male sterility and quantitative female fertility (Fig 1).

256
257 **Confirmation of SDR in additional crosses**

258 In order to examine the species-wide relevance of the HM×SAL results, we tested
259 whether sex mapped to the SDR in two independent crosses. In the EUR cross, we genotyped

260 SDR-vicinity amplicons of 10 male-fertile and 10 male-sterile offspring. We observed 4 Av-m
261 segregating sites and 3 Av-p segregating sites in EUR (S2 Table; Fig S1). Similarly, in the PTR
262 cross we genotyped SDR-vicinity amplicons of 6 male-fertile offspring, 11 male-sterile
263 offspring, and 3 offspring of unknown sex phenotype. We observed 12 Av-m segregating sites
264 and 4 Av-p segregating sites in PTR (S2 Table; Fig S1). Among both EUR and PTR, all Av-m
265 SNPs in the SDR vicinity showed a perfect match to sex, with no observed recombinants.

266

267 **Recombination**

268 In order to calculate recombination rates along the entire ZW sex chromosome (VI-Av-m
269 and VI-Av-p) and compare them to genome-wide patterns, we re-examined all linkage groups in
270 the published *F. chiloensis* target capture maps [45]. Among all linkage groups we observed 747
271 maternal recombination events and 731 paternal recombination events, suggesting a genome-
272 wide recombination rate of 2.5 cM/Mb given a genome size of approximately 700 Mb [52]. In
273 order to examine variation in recombination rates across the genome, we calculated rates for 138
274 segments of 5-10Mb. Recombination rates varied from 0 to 7.0 cM/Mb (median = 2.3, mean =
275 2.5, standard deviation = 1.4; Fig 4). There was no significant difference between maternal and
276 paternal recombination rates genome-wide (Wilcoxon rank sum test, $p > 0.1$; Fig 4).
277 Remarkably, among the 56 linkage groups, VI-Av-m (the ZW linkage group) had the second-
278 highest observed recombination rate of 3.3 cM/Mb, only slightly exceeded by the rate of 3.4
279 cM/Mb observed on I-Av-p (S6 Table). A relatively high rate appears consistently across this
280 entire VI-Av-m linkage group (Fig 4 pink circle) and is notably higher than the rate in all other
281 VI linkage groups (Fig 5). Based on Fvb chromosome lengths, the VI-Av-m linkage group is

282 estimated to constitute 2.3% of the *F. chiloensis* genome, suggesting an expected 34
283 recombination events, a prediction significantly exceeded by the observed 53 recombination
284 events on VI-Av-m (53:1425 vs. 34:1444 recombination events; $\chi^2 = 4.3$, $p < 0.05$). Conversely,
285 VI-Av-p (the ZZ linkage group) had one of the lowest recombination rates at 1.7 cM/Mb (Fig 4
286 blue circle), lower than all other VI linkage groups (Fig 5), and with only 5 out of 56 linkage
287 groups showing less recombination (S6 Table). Thus, recombination rate is nearly 2-fold higher
288 between ZW chromosomes than between ZZ chromosomes (53:27 vs. 40:40 recombination
289 events, $\chi^2 = 4.3$, $p < 0.05$).

290

291 **Fig 4. Genome-wide recombination rates compared to ZW rates.** The *F. chiloensis* target capture linkage maps
292 were divided into sections of 5-10Mb, free from any known rearrangements. Recombination rate was calculated for
293 each section, as shown in this histogram of maternal (pink) and paternal (light blue) recombination rates. Symbols
294 indicate maternal and paternal recombination rates across the entire VI-Av linkage group (circles; ZZ or ZW), across
295 the SDR vicinity from Fvb6_37.38–38.29 (diamonds), and across the SDR from Fvb6_37.38–37.71 Mb (triangles).
296 Recombination is notably higher in the mother than in the father across VI-Av, but this pattern reverses at the SDR.

297

298 **Fig 5. Recombination events across all eight VI linkage groups.** Markers in each linkage group are plotted with
299 physical Fvb reference genome position on the x-axis and centimorgan position on the y-axis. Recombination rates
300 are therefore indicated by the slopes of the lines, as illustrated by the example slopes in the figure legend. Lines are
301 color-coded based on subgenome, and are solid for maternal linkage groups and dashed for paternal linkage groups.
302 The SDR is shown as a dark red box. For ease of visualization, markers showing radical rearrangements relative to
303 the reference genome (<5% of all markers) have been removed. The VI-Av-m linkage group harboring the SDR has
304 the highest recombination rate across the entire chromosome, while the VI-Av-p linkage group has the lowest
305 recombination rate.

306

307 In order to test for recombination suppression at the SDR, we calculated maternal and
308 paternal recombination rates from the amplicon data. Across the 1Mb of the SDR vicinity in
309 which we observed segregating sites in amplicons, recombination rates were nearly identical on
310 VI-Av-m and VI-Av-p (2.9 cM/Mb maternal, 2.8 cM/Mb paternal; Fig 4 diamonds). However, in
311 the 330kb between Fvb6_37.378-37.708Mb, containing the entire male function region and most
312 of the female function region, recombination was notably lower on VI-Av-m relative to VI-Av-p
313 (Fig 4 triangles). Specifically, there are six Av-m recombination events in this window (1.5
314 cM/Mb) compared to sixteen Av-p recombination events (4.1 cM/Mb) (6:1209 vs. 16:1180
315 recombination events; $\chi^2 = 4.7$, $p < 0.05$). In comparison to genome-wide rates, the
316 recombination rate at the SDR in VI-Av-m is lower than average, but not significantly so (given
317 2.5 cM/Mb mean rate, expect 10 recombination events between Fvb6_37.378-37.708Mb, 6
318 observed; $\chi^2 = 2.6$, $p > 0.1$), and well within the range observed elsewhere in the genome (30%
319 quantile; Fig 4). Likewise, the recombination rate at the SDR in VI-Av-p is higher than the
320 genome-wide average but not an outlier. Unfortunately, we did not observe SNPs at both
321 boundaries of this interval in any other homeolog, and therefore we cannot directly compare
322 recombination rates among subgenomes specifically at the SDR.

323

324 **Divergence between W and Z**

325 In order to assess sequence divergence between W and Z chromosomes, we evaluated
326 SNPs in the vicinity of the SDR in the three crosses. In each of these, we classified SNPs as

327 either in coupling with male sterility/female fertility (W-specific), in repulsion in the mother, or
328 segregating in the father (Fig S1). In all three crosses, we observed more SNPs that differentiate
329 Z from W (52 total, not correcting for shared SNPs among crosses) than SNPs which differ
330 between two Z chromosomes (31 total, not correcting for shared SNPs among crosses).
331 Specifically, on VI-Av in HM×SAL, we observed 18 SNPs in coupling, and 18 SNPs in
332 repulsion, with male sterility/female fertility, and 9 and 15 SNPs on each of the paternal Z
333 haplotypes. On VI-Av in EUR, we observed 2 SNPs in coupling, and 2 SNPs in repulsion, with
334 male sterility/female fertility, and 0 and 3 SNPs on each of the paternal Z haplotypes. On VI-Av
335 in PTR, we observed 7 SNPs in coupling, and 5 SNPs in repulsion, with male sterility/female
336 fertility, and 0 and 4 SNPs on each of the paternal Z haplotypes. Intriguingly, the highest
337 concentration of W-specific SNPs occurred within the male-sterility region, specifically in a
338 143kb “high W divergence” window between 37.565-37.708Mb, with 10 SNPs in coupling with
339 male sterility/female fertility in HM×SAL, 4 in PTR, and 1 in EUR. For HM×SAL, the W-
340 specific divergence (SNPs in coupling out of all sequenced sites) in the high W divergence
341 window is 0.39%, substantially higher than both the 0.07% of sites segregating on a single Z
342 haplotype in this window (observe 10:5 W:Z, expect 3.75:11.25, $\chi^2 = 4.8$, $p < 0.05$), and the
343 0.06% W-specific divergence observed across all amplicons outside of this high-divergence
344 window. The higher SNP counts observed in the HM×SAL cross relative to EUR and PTR
345 crosses may be due to the parents of the former originating in different populations (and thus
346 fewer SNPs segregating in both parents, which we ignored in our mapping methodology), as well
347 as the much larger offspring sample size (and thus higher power to map SNPs even when a large
348 proportion of offspring have missing genotypes). Nevertheless, a single G/C SNP, which occurs

349 within the high divergence window at position Fvb6_37594072, was in coupling with male
350 sterility/female fertility (W allele = C; Z allele = G) in all three crosses (Fig 3; Fig S1).

351

352 **Association between genotype and sexual phenotype in unrelated plants**

353 In order to identify SNPs in linkage disequilibrium with the causal sex gene(s), we
354 examined genetic diversity at SDR vicinity amplicons in 22 unrelated plants, 10 male-sterile and
355 12 male-fertile (the six parents of the crosses plus 16 additional plants). A single SNP showed a
356 near-perfect correlation with sex: the same G/C SNP at Fvb6_37594072 for which the C allele
357 was in coupling with male sterility/female fertility (W) in all three crosses (Fig S1). The SNP
358 was heterozygous (G/C) in 9 out of 10 male-sterile plants (ZW), and homozygous (G/G) in 11 of
359 12 male-fertile plants (ZZ). Due to its widespread and consistent association with sexual
360 phenotype, we designated this SNP the “universal marker” (Fig 3; Fig S1). Four additional SNPs
361 (Fvb6_37565581, Fvb6_37565641, Fvb6_37567599, and Fvb6_37567962; Fig S1), all within
362 the high W divergence window of the male function region, showed a weaker association with
363 sex, but all were heterozygous in 80-90% of male-sterile plants and homozygous in 60-70% of
364 male-fertile plants.

365

366 **Discussion**

367 Our study of incipient sex chromosomes in octoploid *F. chiloensis* illuminates how
368 recombination rates may first begin to adjust in response to sex linkage. Sex chromosomes are
369 characterized by having atypical recombination patterns relative to autosomes [16]. These unique

370 recombination dynamics are the evolutionary basis for the other unusual features of sex
371 chromosomes, such as heteromorphy, rapid molecular evolution, degradation, and determination
372 of hybrid incompatibility [53]. Recombination rates across the genome are determined by several
373 factors: crossover motifs and the associated epigenetic and chromatin modifications, sequence
374 divergence among sister chromatids including rearrangements such as inversions, and specific
375 genes that dictate pairing compatibilities [54],[55]. Selection pressures to rapidly adjust
376 recombination rates for nascent sex chromosomes are similar to those facing neopolyploids
377 undergoing diploidization [54], and both processes may involve similar molecular mechanisms
378 and a similar period of adaptation during which recombination patterns are not optimal. Here we
379 have examined recombination in the youngest and least differentiated plant ZW chromosome yet
380 described.

381

382 **A small SDR**

383 In contrast to most older sex chromosomes, we do not observe a wide (>1Mb) SDR
384 characterized by suppressed recombination. In fact, across most of the SDR vicinity targeted by
385 amplicon sequencing, recombination rates were typical and nearly identical between VI-Av-m
386 and VI-Av-p (Fig 3). Both male and female function mapped to a single 280kb chromosomal
387 region within the region first identified by Goldberg et al. [27] at the distal end of VI-Av-m. The
388 maximum possible extent of suppressed recombination occurs within a 330kb window centered
389 on this SDR. Observed VI-Av-m recombination in this window is less than half that of VI-Av-p.
390 However, the VI-Av-m recombination rate is not unusually low relative to autosomal rates. The
391 fact that neither male nor female function was perfectly correlated with the SDR suggests that

392 other unlinked loci or environmental effects may also influence sex in *F. chiloensis*. This is
393 especially likely for female function, a quantitative trait for which the SDR explains 74% of
394 variation, but also one known to be highly environmentally labile in other *Fragaria* [56]. Such
395 minor contributors to female function variation have also been seen in the subdioecious *Fragaria*
396 *virginiana* which has a major SDR [11], and are known to segregate in the natural hybrid *F.* ×
397 *ananassa* subsp. *cuneifolia* [57]. Male function in contrast was almost perfectly determined by
398 the SDR, with <1% of HM×SAL offspring showing a mismatch, suggesting that any other
399 factors affecting the propensity to produce pollen are negligible.

400 We cannot determine whether male and female function are controlled by two closely
401 linked genes, or both by the same gene. This question is relevant to recombination patterns
402 because the primary theoretical basis for recombination suppression assumes two genes [19].
403 Presumably a single gene initially controlled a single phenotype such as male function,
404 especially given the observed gynodioecy in the closely related *Fragaria vesca* subsp. *bracteata*
405 [58] (but see [44]). Under the classic model of sex chromosome evolution [18],[19], a second
406 linked mutation occurs such that there are two distinct linked genes controlling male and female
407 function. Recombination between these genes produces neuters, prompting strong selection for
408 recombination suppression. In *F. chiloensis*, the two-locus model would require a remarkably
409 small physical distance between the two loci (within the predicted 280kb SDR), but this could
410 arise either coincidentally or else via adaptive translocation of the second locus in order to
411 achieve tight linkage. Because baseline recombination should only occur rarely within a 280kb
412 region (fewer than 1% recombinant offspring at the 2.5 cM/Mb genomic mean rate), selection for
413 additional recombination suppression would not be particularly strong. Although recombination
414 between loci controlling male and female function would theoretically produce neuters [11],[18],

415 we observe only 7 out of 619 HM×SAL offspring showing both male and female sterility, none
416 of which show recombination on VI-Av-m, and four of which produced only 1-2 flowers, and
417 thus may have failed to fruit by chance. Alternatively, there may be only a single sex determinant
418 at the SDR, as proposed for other dioecious systems in which only a single regulator of sex has
419 been identified [59],[60]. A single sex-determining gene for *Fragaria* was proposed by Ahmadi
420 and Bringhurst [61], although their genus-wide model was too simple given the distinct sex loci
421 subsequently observed among species [11],[27],[43],[44],[48]. Ancestrally, individuals with ZZ
422 genotypes may have been universally hermaphrodites, as in gynodioecious species with
423 dominant male sterility allele(s) such as *F. vesca* subsp. *bracteata* [43],[44]. Variation in female
424 function among male-fertile individuals could have been influenced by gene(s) anywhere in the
425 genome, not necessarily on VI-Av. If males had higher fitness than hermaphrodites [62], alleles
426 conferring female sterility (but only in male-fertile individuals) would increase in frequency or
427 even fix, leading to the highly dioecious condition observed in *F. chiloensis* even without new
428 sterility mutations on VI-Av. Selection could favor linkage of female fertility modifiers to the
429 SDR, but such selection would be weak if these mutations had little phenotypic effect in females
430 [63]. If a single gene controls both male and female function in *F. chiloensis*, there would only
431 be selection for recombination suppression if other linked genes had alleles with differential
432 fitness between sexes, i.e., antagonistic selection [15].

433 Although the causal sex gene(s) remain unidentified, as in most dioecious plants, several
434 promising candidates are apparent among the 70 known genes in the SDR (S5 Table). One gene
435 encodes a mitochondrial-targeted pentatricopeptide repeat protein, a molecular family commonly
436 implicated in male fertility restoration when cytoplasmic genes cause sterility [64]. There are two
437 methyltransferases, another gene family which may control sex in other plants [32]. A cluster of

438 five cystinosin homologs, out of only six in the entire Fvb genome, occurs in this window.
439 Cystinosin mutations cause male sterility in humans [65], indicating a possible role for cystine
440 transport in *Fragaria* sex function as well. Although we can't determine how close the universal
441 marker is to the causal genes(s), there are 13 genes within 25kb of this SNP, including four F-
442 box proteins, an abhydrolase domain-containing protein, and a glycerol-3-phosphate
443 dehydrogenase. An exciting future direction will be to test SDR genes for sexual function or
444 sexually antagonistic alleles.

445

446 **Recombination at the PAR**

447 In addition to suppressed recombination at the SDR, sex chromosomes frequently show
448 elevated recombination in the PAR [15]. In the case of *F. chiloensis*, the PAR represents over
449 99% of the 39Mb VI-Av chromosome. Thus the PAR recombination rate is approximated by
450 examining the entire chromosome, over which VI-Av-m recombination is nearly twice as high as
451 VI-Av-p recombination. Recombination rates are not as high on the other *F. chiloensis* VI
452 linkage groups, and in fact are lower among all 56 *F. virginiana* linkage groups [45], suggesting
453 that the high VI-Av-m rate in *F. chiloensis* is newly evolved. Although elevated PAR
454 recombination has been attributed to compensation for suppressed SDR recombination [15], in *F.*
455 *chiloensis* the PAR greatly over-compensates for the SDR. Thus, the adaptive value of this
456 elevated recombination rate, if any, does not appear to involve compensation. Instead, perhaps
457 there is a benefit for certain alleles to recombine away from the SDR, at least in the early stages
458 of sex chromosome evolution. One intriguing possibility is that the effective population size of
459 the W chromosome is relatively low due to fluctuating, male-biased sex ratios, which are

460 common in dioecious plants [66], and which could explain the high W-specific divergence.
461 Population proportions of male-sterile plants may occasionally decrease under ecological
462 conditions that favor hermaphrodites, which could lead to accumulation of deleterious mutations
463 on the W, unless these are eliminated by recombination. Thus, high recombination in the Z-W
464 PAR could be favored as a way to avoid Muller's ratchet [67].

465 Although examination of recombination rate is standard in studies of sex chromosomes
466 [18], statistical detection of recombination suppression or elevation is not always
467 straightforward. Until recently, most studies of plant recombination heterogeneity lacked a
468 physical map (e.g. [68]-[70]), and thus could only compare the relative densities of markers at
469 linkage map positions. Our approach of integrating linkage maps with reliable reference
470 sequences, which is increasingly common [29],[34],[71], affords much more precision.
471 Nevertheless, such recombination estimates carry several caveats. The first caveat is the
472 challenge of designating an appropriate control. For example, to test if the recombination rate in
473 an SDR is unusual, it could potentially be compared to the orthologous region in the
474 homogametic parent, the PAR, the homeologous chromosomes, the autosomes, or the genomes
475 of outgroup species, with variable results [72],[73]. By considering all of these comparisons, we
476 can achieve a more nuanced view of recombination heterogeneity. For example, although
477 maternal recombination is lower at the SDR than the PAR (Fig 4), this is due at least as much to
478 elevated recombination at the PAR as to suppressed recombination at the SDR. A second caveat
479 to all our recombination analyses is that physical distances are estimated from the Fvb reference
480 genome. Major rearrangements between *F. chiloensis* and *F. vesca* subsp. *bracteata*, such as
481 large insertions or deletions, would affect our estimates. However, we minimized the effects of
482 this limitation in several ways: by identifying and avoiding rearrangements in the target capture

483 map, by focusing on the subgenome (Av) which is most closely related to *F. vesca* subsp.
484 *bracteata*, and by making direct comparisons between maternal and paternal maps under the
485 assumption that most large rearrangements would be present in both parents. Thus, our
486 conclusions are robust to both of these caveats.

487

488 **Evolutionary dynamics at the SDR vicinity**

489 The *F. chiloensis* SDR represents the narrowest fine-mapping of any *Fragaria* sex locus
490 to date. It is distinct from the *F. virginiana* subsp. *virginiana* SDR which also occurs on a VI
491 chromosome [11],[48]. Furthermore, the *F. chiloensis* SDR is distinct from one of the male-
492 function-influencing loci *F. vesca* subsp. *bracteata*, the *Rr* locus which intriguingly occurs less
493 than 1 Mb away at Fvb6_34.839-36.607Mb [44], but confers recessive male sterility (*rr*).
494 Perhaps the VI chromosome, especially the distal end between Fvb6_34-38Mb, is particularly
495 suited to controlling sex phenotype [11]. The myriad sex loci among closely related *Fragaria*
496 species suggest a dynamic evolutionary process that may involve repeated independent sterility
497 mutations, gene translocations, and/or shifting genetic control of phenotype. In fact, turnovers
498 driven by sexually antagonistic genes and/or escape from mutational load also can produce “ever
499 young” small SDRs [74] and can account for XY to ZW transitions as well. These are expected
500 to be particularly common in species with undifferentiated sex chromosomes, and some
501 autosomal pairs are more likely than others to be recruited [74],[75]. Such dynamics have been
502 proposed to be responsible for the variation in position of the SDR and heterogamety in willows
503 [60].

504 In contrast to the variable basis of sex determination between species, the SDR is highly
505 consistent within *F. chiloensis*. The same SDR was identified in two additional *F. chiloensis*
506 crosses from populations up to 1000 km away, suggesting it may be the most common, or only,
507 SDR in this species, at least in North America. A single “universal marker” was in coupling with
508 male sterility/female fertility phenotype in all three crosses, and this SNP also showed near-
509 perfect association with sex across a set of unrelated plants. Of the two exceptions, one plant was
510 the sole specimen from South America which may have a distinct sex determining mechanism.
511 The other was from the same population as one of the crosses (PTR), suggesting either that the
512 SDR does not perfectly control sex in all cases, or that the universal marker is not in perfect
513 linkage disequilibrium with the causal gene(s). One consequence of recombination suppression
514 should be that a W-specific haplotype behaves as a single unit in population genetics, with
515 multiple SNPs in linkage disequilibrium with sex. The fact that only a single universal marker
516 was observed, despite our sequencing ~2% of the 280kb SDR, suggests that there are few SNPs
517 (less than 100) showing such high linkage disequilibrium with sex. In turn, this observation
518 suggests that the true SDR may be substantially smaller than the 280kb mapped region, although
519 we cannot definitively demonstrate this.

520 We observe a particularly high concentration of maternally-heterozygous SNPs in a small
521 genomic section corresponding to the second half of the SDR (Fig 3, Fig S1). Thus, divergence
522 between W and Z is particularly high in this window, especially for SNPs in coupling with male
523 sterility/female fertility and therefore W-specific within crosses. Note that, other than the
524 universal marker, these SNPs are not W-specific across populations, but some may be W-
525 specific within populations. Our study design doesn’t allow us to examine divergence shared by
526 all Z chromosomes but not the W, since such Z-specific SNPs will occur in both parents and thus

527 will not segregate in the offspring. Female-specific mutations could accumulate at the SDR for
528 several reasons: suppressed recombination, selection against recombinants, or low effective
529 population size at the SDR due to fluctuating sex ratios, such that deleterious mutations are not
530 purged by selection [29],[32]. As discussed above, the accumulation of deleterious W-specific
531 mutations could potentially explain why high recombination in the PAR is adaptive. These
532 processes could lead to even greater Z-W differentiation. Alternatively, given that heteromorphic
533 sex chromosomes seem to have only rarely become established in dioecious flowering plants,
534 these may not necessarily evolve in *F. chiloensis*, and Z-W divergence could remain subtle
535 indefinitely, especially if recombination eliminates W-specific changes.

536

537 **Conclusions**

538 We have characterized an incipient ZW sex chromosome in a dioecious wild strawberry,
539 pinpointing a single SDR controlling both male and female function within a narrow genomic
540 window, and examining recombination and divergence patterns in Z-Z and Z-W pairs. Along
541 with other recent studies of homomorphic plant sex chromosomes [20],[27-34], this work
542 suggests that small, modestly divergent SDRs may be typical of many dioecious plants. By
543 extensively analyzing recombination, this study reveals rate heterogeneity patterns both expected
544 and surprising, which could nonetheless be typical of such young sex chromosomes. Our work is
545 also novel in that *F. chiloensis* has a ZW system and that it is a higher-order polyploid, thus
546 extending our understanding of small plant SDRs beyond XY diploids. These subtle plant SDRs
547 may be affiliated with relatively low sexual dimorphism, and thus little selection pressure on
548 genes to become tightly linked to sex [38], consistent with few observed sex differences in *F.*

549 *chiloensis* [50] (but see [8]). When compared with classic, highly heteromorphic sex
550 chromosomes of other taxa [22],[23],[71], our results speak to the diversity of genomic patterns
551 in sexual species. However, even when the SDR represents a tiny fraction of the genome, linkage
552 to sex may have important consequences for loci all along the sex chromosome, as exemplified
553 here by the elevated PAR recombination rate.

554 The evolutionary processes that generate and modify sex chromosomes across taxa are
555 now partially understood, but remain to be fully characterized. Theoretical assumptions, like that
556 elevated PAR recombination serves to compensate for suppression at the SDR, or that SDRs
557 evolve from two linked genes controlling male and female function, may not hold true for all
558 taxa. The patterns of recombination, divergence, and linkage disequilibrium observed in the *F.*
559 *chiloensis* ZW chromosomes can be further explored by measuring fitness, gene function, and
560 population genetic parameters. This species thus presents an ideal opportunity for continued
561 study of the emergence of sex chromosomes.

562

563 **Materials and Methods**

564 **Samples**

565 The primary cross examined in this study (here designated HM×SAL) represents an
566 expanded set of F1 offspring from an intraspecific cross involving a female *F. chiloensis* subsp.
567 *lucida* (GP33) and a hermaphroditic *F. chiloensis* subsp. *pacifica* (SAL3) used in previous work
568 [27]. The maternal parent was obtained from the USDA National Clonal Germplasm Repository
569 (accession no. PI 612489; ‘HM1’) which was originally collected from Honeyman Memorial

570 State Park, Oregon (43.93N, 124.11W). To emphasize its population of origin, shared by several
571 other plants in the current study (S3 Table), we here use the designation of the maternal parent as
572 HM1 (although note previously this cross was referred to as GP33xSAL [27]). The paternal
573 parent was collected from Salishan, Oregon (44.91N, 124.02W) and is a low fruit-producing
574 hermaphrodite (10% of hand-pollinated flowers yielded fruits in the greenhouse). We hand
575 pollinated pistillate flowers of HM1 with the pollen from SAL3. We planted a total of 1695
576 seeds in sets across five years (between 2009 and 2015) and 75% of which germinated. We
577 transplanted ~ 2-month old seedlings into 3-inch-square pots filled with a 2:1 mixture of Fafard
578 #4 (Conrad Fafard) and sand. In the first growing period after germination in each year the plants
579 received a total of 513 mg of granular Nutricote 13:13:13 N:P:K fertilizer (Chisso-Asahi
580 Fertilizer). All plants were grown under mild temperatures (15°/20° night/day) and 10- to 12-hr
581 days throughout the majority of the flowering period. To initiate flowering plants were exposed
582 to cooler temperatures (8°/12° night/day) with an 8 hr day with low light. Additional liquid
583 fertilizer and pest control measures were applied as needed to maintain the health of the plants to
584 flowering.

585 We also examined the parents and F1 offspring of two other independent *F. chiloensis*
586 crosses, in order to test the universality of the location of the SDR identified in HM×SAL and to
587 identify SNPs universally in coupling with male sterility/female fertility (i.e., on the W haplotype
588 of the SDR). The parents of the first cross (EUR) were a female (EUR13) and a male (EUR3; 0%
589 fruit set) *F. chiloensis* subsp. *lucida* collected from Eureka, California (40.762 N, 124.225 W).
590 The parents of the second cross (PTR) were a female (PTR14) and a low fruit-producing
591 hermaphrodite (PTR19; 10% fruit set) *F. chiloensis* subsp. *lucida* collected from Point Reyes,
592 California (38.0683 N, 122.971 W). We raised 105 and 65 F1 offspring from the two crosses,

593 respectively, following the same planting and growth regimes as in HM×SAL cross. As the goal
594 of these crosses was validation of the sex-linked SNP results from the HM×SAL cross, rather
595 than fine-mapping, we examined substantially fewer offspring than for HM×SAL. Twenty
596 offspring from each cross are studied further here.

597 In addition, we examined 16 unrelated plants from six populations (the four source
598 populations of cross plants and two other populations) across the geographic range of *F.*
599 *chiloensis* (S3 Table). The plants were collected from the wild as clones or obtained from the
600 National Clonal Germplasm Repository and raised under the same planting and growth
601 conditions as described above.

602

603 **Sex phenotyping**

604 We scored plants of HM×SAL for both male and female function following Spigler et al.
605 [11]. We scored male function on at least two flowers per plant two separate times. Male
606 function was scored as a binary trait: “male fertile” if the plant had large, bright-yellow anthers
607 that visibly released pollen, and “male sterile” if the plant had vestigial white or small, pale-
608 yellow anthers that neither dehisced nor showed mature pollen. Any anthers that were in
609 question were examined microscopically for the presence of mature pollen. To ensure full
610 potential fruit set, we hand pollinated all plants three times per week with outcrossed pollen. We
611 then estimated female fertility for each individual as the proportion of flowers that produced fruit
612 by dividing the total number of fruits by the total number of pollinated flowers produced as in
613 Spigler et al. [11]. In order to measure to extent to which male sterility co-occurs with female

614 fertility, we calculated the association between male function and female function using simple
615 linear regression [76]. Because female fertility may be influenced by plant size (here estimated
616 as the total number of flowers [or buds] produced), we also included total flower number as a
617 second independent variable in multiple regression [76]. In QTL analysis, female function was
618 examined as a continuous quantitative trait. For progeny in the EUR and PTR crosses and the
619 unrelated individuals male function was scored similarly as HM×SAL, but female function was
620 scored only as binary.

621

622 **DNA extraction and quantification**

623 We extracted DNA from fresh or dry leaf tissue. Fresh tissue extractions using a modified
624 CTAB method were done on 42 F1 offspring from the 2009 mapping population for target
625 capture sequencing to construct initial high density linkage map, as described previously [45].
626 For the remaining HM×SAL offspring, we collected leaf tissue from seedlings or adult plants
627 and stored on silica gel. Similarly, for the EUR and PTR *F. chiloensis* crosses, we collected,
628 dried and extracted DNA from leaves of a total of 20 offspring representing 10 females and 10
629 pollen-bearing morphs (hermaphrodites or males) from each cross. To extract DNA from dry
630 tissue samples, we used the Norgen biotek plant/fungi high-throughput 96 well DNA isolation kit
631 (Norgen Biotek, ON, Canada) and also used DNA extraction service provider Agbiotech Inc
632 (CA, USA). We added an additional 100ul 10% SDS and 10ul β-mercaptoethanol to the lysis
633 buffer to improve DNA yield from all the dry tissue samples. The final DNA elution was sodium
634 acetate/ethanol precipitated to wash and concentrate the DNA. Picogreen assays were performed
635 using a Tecan plate reader to measure DNA concentration for each sample, and we diluted DNA

636 to 50ng/ul using DEPC treated water to use in microfluidics PCR on the Fluidigm access array
637 system (see below).

638

639 **Target capture mapping**

640 We previously described a target capture linkage map of 2542 segregating markers
641 generated using 42 HM×SAL offspring [45]. All markers align to a distinct position in the
642 haploid *F. vesca* reference genome (v. 2.0, here designated “Fvb” as in [45]), and also have a
643 linkage map position in cM on a paternal (“p”) or maternal (“m”) linkage group pertaining to one
644 of the four octoploid subgenomes (Av, B1, B2, or Bi). In order to map sex phenotypes, we first
645 coded male function as a binary trait (male sterile=0; male fertile=1) and added it to the linkage
646 map with OneMap [77], as in Tennessen et al. [43]. Because female function is defined as a
647 proportion between 0 and 1, rather than a binary trait, we identified female function quantitative
648 trait locus (QTL) using R/qtl [76],[78]. Specifically, we first used the scanone option to identify
649 all possible female function QTL, using a minimum LOD threshold of 3. Then we checked
650 whether more than one additive QTL was independently supported using the scantwo option; a
651 model with two additive QTL would need a LOD at least 3 greater than the LOD of the single
652 best QTL in order to be significant. The region of the Fvb genome where both male function and
653 female function QTL mapped, presumably harboring the SDR and possibly also adjacent
654 portions of the PAR, was designated the “SDR vicinity” and examined with additional
655 genotyping as described below.

656 In order to estimate genome-wide recombination rates, we first re-examined the
657 published linkage maps of HM×SAL [45] to confirm all recombination events by eye and
658 eliminate putative recombination events that could be caused by genotyping error. As in previous
659 studies [43],[45], a pair of adjacent recombination events in the same individual on either side of
660 a single marker was considered to be a genotyping error rather than a real double recombination
661 event. We also identified all inconsistencies in marker order when compared with the Fvb
662 reference genome. If an inconsistency could be explained by a single incorrect genotype, it was
663 attributed to genotyping error, otherwise it was considered to be a genomic rearrangement (either
664 a genome assembly error or a real translocation, the distinction is irrelevant here). We assumed
665 that physical distances on the octoploid chromosomes could be approximated by Mb distances in
666 the Fvb reference genome, and thus we estimated recombination rates genome-wide and per each
667 linkage group as cM/Mb. Although the 0.7 Gb octoploid *Fragaria* genome has likely undergone
668 some gene loss and other rearrangements relative to the 0.2 Gb diploid reference [45],[52], these
669 discrepancies should have a minimal effect when comparing relative rates among linkage groups,
670 and should also be rarest on the Av subgenome containing the sex chromosome because it
671 originates from *F. vesca* subsp. *bracteata*. In order to further examine variation in recombination
672 rate across the genome of *F. chiloensis*, we divided all 56 linkage groups in the genome into
673 segments of 5-10Mb that were free from rearrangements, and calculated recombination rates for
674 each of these segments.

675

676 **Amplicon generation and sequencing**

677 In order to fine-map the SDR vicinity and examine recombination rates, we genotyped
678 sites in SDR vicinity using Illumina sequencing of targeted amplicons [79]. The Fluidigm
679 microfluidic approach is an effective method for mapping SNP markers in a large sample of
680 polyploids [80],[81], and by sequencing amplicons we can unambiguously assign markers to a
681 genomic position. We performed sequencing in three sequential rounds, refining the combination
682 of targeted amplicons each time based on amplicon performance and fine-mapping results (S7
683 Table; S8 Table). Some samples were included in multiple rounds due to poor-quality genotypes
684 or in order to further fine map recombinants. Initially, we designed primers for 48 amplicons of
685 approximately 300-600bp (we found that larger amplicons performed poorly), with a Fvb
686 reference genome position within the SDR vicinity. Most amplicons (41) contained at least one
687 SNP (on any subgenome) identified in the target capture map. We used the Fluidigm 48.48
688 Access Array IFC (Integrated Fluidic Circuits) to generate amplicons in parallel. These steps
689 were performed by IBEST at the University of Idaho. The forward and reverse primers were
690 attached with common sequence tags (CS1 & CS2) to enable the addition of P5 and P7 Illumina
691 adapters along with dual index multiplex barcodes during the four primer PCR reactions. All
692 primer pairs were validated using DNA from parent HM1 to verify the expected product size and
693 ascertain the on-target products to account for a minimum of 50% of the total yield (by mass) for
694 each primer pair. For validation PCR and optimization we followed the Fluidigm Access Array
695 System user guide for Illumina (<https://www.fluidigm.com/documents>; Access Array 48.48-4-
696 primer-amplicon-tagging). We used the Agilent bioanalyzer (Agilent Technologies Inc.) to
697 determine the expected amplicon size and yield. We redesigned primers to meet the validation
698 criteria as necessary. After validation, we generated amplicons in microfluidic reactors, tagging
699 each amplicon with unique dual index barcodes. We multiplex sequenced 48 pools of amplicons

700 (one per individual) in 10-12 access array plates on one-half lanes of the Illumina MiSeq,
701 yielding 300-bp paired-end reads. For the first round we sequenced 478 HM×SAL offspring and
702 the two parents. For the second round of sequencing, we retained 19 of the original 48 primer
703 pairs and replaced 29 with newly designed primer pairs. We used these to sequence 469
704 HM×SAL offspring, the two HM×SAL parents, and the parents and 20 offspring each from the
705 EUR and PTR crosses. For the third round of sequencing, we retained 39 primer pairs and
706 replaced 9 with newly designed primer pairs, and we used these to sequence 545 HM×SAL
707 offspring, the two HM×SAL parents, the same EUR and PTR individuals from the second round,
708 and 18 additional unrelated plants (16 of which yielded useable genotypes and were analyzed
709 here). In total, 1302 unique plants were included in amplicon sequencing. Including the target
710 capture samples, a total of 1274 HM×SAL offspring were genotyped.

711

712 **Amplicon genotyping and fine mapping**

713 We called genotypes using the POLiMAPS approach [45]. In brief, we first processed
714 Illumina reads with dbcAmplicons (<https://github.com/msettles/dbcAmplicons>), trimmed them
715 with Trimmomatic [82], aligned them to the amplicon regions extracted from Fvb reference
716 genome with BWA [83], and generated pileup files with SAMtools [84]. We called genotypes in
717 the pileup file using the same coverage criteria as in the target capture map [45], i.e. minimum
718 depth of 32, alternate allele must occur in an individual at least twice and at $\geq 2.5\%$ frequency,
719 only SNPs heterozygous in a single parent are considered. However, because sample sizes were
720 larger and there were more missing genotypes than in the target capture map, we adjusted the
721 additional criteria for HM×SAL amplicons, allowing up to 200 missing genotypes per site and

722 requiring 40 observations each of homozygotes and heterozygotes for a SNP to be called as real.
723 For EUR, PTR, and the set of unrelated plants, all with much smaller sample sizes, we allowed
724 up to 10 missing genotypes and required 4 observations each of homozygotes and heterozygotes.
725 We converted genotypes to OneMap format and generated linkage maps in OneMap with a LOD
726 criterion of 3.

727 We identified recombination events and used these to estimate recombination rates in the
728 SDR vicinity and to fine map sex QTL. Because male function showed a near-perfect match to
729 genotype, and the few exceptions were not recombinants in the SDR vicinity, we simply defined
730 the male function region as the section of chromosome between the closest recombination events
731 both upstream and downstream that caused mismatches between genotype and male function.
732 Because female function is a continuous trait showing a weaker correlation with genotype, we
733 calculated LOD scores for all sites in the SDR vicinity. We also calculated the correlation
734 between genotype and female function across the SDR vicinity and used the R/cocor package
735 [75],[85] to compare these correlations and thus to define the female function region as the
736 region in which correlations were not significantly different from that at the site with the best
737 LOD score. Because male function could thus be more precisely mapped than female function,
738 we considered the male function region to comprise the maximum potential extent of the SDR.
739 We examined genes within the male function region by consulting both the original annotation of
740 the Fvb genome [45],[86] and a recent re-annotation by Darwish et al. [51]. As with the whole-
741 genome analysis from the target capture map, we estimated recombination rate as cM/Mb, with
742 physical distance estimated from the Fvb reference genome. This assumption is particularly
743 justified for the Av subgenome because it originates with *F. vesca* subsp. *bracteata* [45].

744

745 **Acknowledgements**

746 The authors thank C. Kustek, K. Mazzaferro, L. Stanley, K. Schuller, R. Dalton, H. Wipf, E.
747 York for greenhouse, field or laboratory assistance, B. Rosa-Neves for help error-checking the
748 linkage maps, the Ashman and Liston labs for comments that improved the manuscript. This
749 work was supported by the University of Pittsburgh, the National Science Foundation (DEB
750 1020523, DEB 1241006, and RET/REU supplements to TLA; DEB 1020271 and DEB 1241217
751 to AL).

752

753 **References**

- 754 1. Bull JJ. Evolution of sex determining mechanisms. Benjamin/Cummings: Menlo Park,
755 CA. 1983.
- 756 2. Charlesworth D, Mank JE. The birds and the bees and the flowers and the trees: lessons
757 from genetic mapping of sex determination in plants and animals. *Genetics*. 2010;186: 9-
758 31.
- 759 3. Haldane JBS. Sex ratio and unisexual sterility in hybrid animals. *J Genet*. 1922;12: 101-
760 109.
- 761 4. Turelli M, Orr HA. The dominance theory of Haldane's rule. *Genetics*. 1995;140: 389-
762 402.

- 763 5. Brothers AN, Delph LF. Haldane's rule is extended to plants with sex chromosomes.
764 Evolution. 2010;64: 3643-3648.
- 765 6. Chang D, Gao F, Slavney A, Ma L, Waldman YY, Sams AJ, et al. Accounting for
766 eXentricities: analysis of the X chromosome in GWAS reveals X-linked genes implicated
767 in autoimmune diseases. PLoS One. 2014;9: e113684.
- 768 7. Evans BJ, Pyron RA, Wiens JJ. Polyploidization and sex chromosome evolution in
769 amphibians. In: Soltis, PS, Soltis, DE, editors. Polyploidy and genome evolution.
770 Springer. 2012. pp 385-410.
- 771 8. Ashman TL, Kwok A, Husband BC. Revisiting the dioecy-polyploidy association:
772 alternate pathways and research opportunities. Cytogenet Genome Res. 2013;140: 241-
773 255.
- 774 9. Zechner U, Wilda M, Kehrer-Sawatzki H, Vogel W, Fundele R, Hameister H. A high
775 density of X-linked genes for general cognitive ability: a run-away process shaping
776 human evolution? Trends Genet. 2001;17: 697-701.
- 777 10. Wilkinson GS, Amitin EG, Johns PM. Sex-linked correlated responses in female
778 reproductive traits to selection on male eye span in stalk-eyed flies. Integr Comp Biol.
779 2005;45: 500-510.
- 780 11. Spigler RB, Lewers KS, Ashman TL. Genetic architecture of sexual dimorphism in a
781 subdioecious plant with a proto-sex chromosome. Evolution. 2011;65: 1114-1126.

- 782 12. Mank JE, Hosken DJ, Wedell N. Conflict on the sex chromosomes: cause, effect, and
783 complexity. *Cold Spring Harb Perspect Biol.* 2014;6: a017715.
- 784 13. Bachtrog D, Mank JE, Peichel CL, Kirkpatrick M, Otto SP, Ashman TL, et al. Sex
785 determination: why so many ways of doing it? *PLoS Biol.* 2014;12: e1001899.
- 786 14. Ohno S. Evolution of the sex chromosomes in mammals. *Ann Rev Genet.* 1969;3: 495–
787 524.
- 788 15. Otto SP, Pannell JR, Peichel CL, Ashman TL, Charlesworth D, Chippindale AK, et al.
789 About PAR: the distinct evolutionary dynamics of the pseudoautosomal region. *Trends*
790 *Genet.* 2011;27: 358-367.
- 791 16. Bergero R, Charlesworth D. The evolution of restricted recombination in sex
792 chromosomes. *Trends Ecol Evol.* 2009;24: 94-102.
- 793 17. Hinch AG, Altemose N, Noor N, Donnelly P, Myers SR. Recombination in the human
794 pseudoautosomal region PAR1. *PLoS Genet.* 2014;10: e1004503.
- 795 18. Charlesworth D. Plant contributions to our understanding of sex chromosome evolution.
796 *New Phytol.* 2015;208: 52–65.
- 797 19. Charlesworth B, Charlesworth D. A model for the evolution of dioecy and gynodioecy.
798 *Am Nat.* 1978;112: 975–997.
- 799 20. Spigler RB, Lewers KS, Main DS, Ashman TL. Genetic mapping of sex determination in
800 a wild strawberry, *Fragaria virginiana*, reveals earliest form of sex chromosome.
801 *Heredity (Edinb).* 2008; 101: 507-517.

- 802 21. Lahn BT, Page DC. Four evolutionary strata on the human X chromosome. *Science*.
803 1999;286: 964-967.
- 804 22. Bernardo Carvalho A, Koerich LB, Clark AG. Origin and evolution of Y chromosomes:
805 *Drosophila* tales. *Trends Genet*. 2009;25: 270-277.
- 806 23. Cortez D, Marin R, Toledo-Flores D, Froidevaux L, Liechti A, Waters PD, et al. Origins
807 and functional evolution of Y chromosomes across mammals. *Nature*. 2014;508: 488-
808 493.
- 809 24. Diggle PK, Di Stilio VS, Gschwend AR, Golenberg EM, Moore RC, Russell JR, et al.
810 Multiple developmental processes underlie sex differentiation in angiosperms. *Trends*
811 *Genet*. 2011;27: 368-376.
- 812 25. Renner SS. The relative and absolute frequencies of angiosperm sexual systems: dioecy,
813 monoecy, gynodioecy, and an updated online database. *Am J Bot*. 2014;101: 1588-1596.
- 814 26. Ming R, Bendahmane A, Renner SS. Sex chromosomes in land plants. *Annu Rev Plant*
815 *Biol*. 2011;62: 485-514.
- 816 27. Goldberg MT, Spigler RB, Ashman TL. Comparative genetic mapping points to different
817 sex chromosomes in sibling species of wild strawberry (*Fragaria*). *Genetics*. 2010. 186:
818 1425-1433.
- 819 28. Fechter I, Hausmann L, Daum M, Sørensen TR, Viehöver P, Weisshaar B, et al. 2012.
820 Candidate genes within a 143 kb region of the flower sex locus in *Vitis*. *Mol Genet*
821 *Genomics*. 287: 247-259.

- 822 29. Wang J, Na JK, Yu Q, Gschwend AR, Han J, Zeng F, et al. Sequencing papaya X and Yh
823 chromosomes reveals molecular basis of incipient sex chromosome evolution. Proc Natl
824 Acad Sci U S A. 2012;109: 13710-13715.
- 825 30. Picq S, Santoni S, Lacombe T, Latreille M, Weber A, Ardisson et al. A small XY
826 chromosomal region explains sex determination in wild dioecious *V. vinifera* and the
827 reversal to hermaphroditism in domesticated grapevines. BMC Plant Biol. 2014;14: 229.
- 828 31. Filatov DA. Homomorphic plant sex chromosomes are coming of age. Mol Ecol. 2015;
829 24: 3217-3219.
- 830 32. Geraldès A, Hefer CA, Capron A, Kolosova N, Martínez-Núñez F, Soolanayakanahally
831 RY, et al. Recent Y chromosome divergence despite ancient origin of dioecy in poplars
832 (*Populus*). Mol Ecol. 2015;24: 3243-3256.
- 833 33. Russell JR, Pannell JR. Sex determination in dioecious *Mercurialis annua* and its close
834 diploid and polyploid relatives. Heredity (Edinb). 2015;114: 262-271.
- 835 34. Zhang Q, Liu C, Liu Y, VanBuren R, Yao X, Zhong C, et al. High-density interspecific
836 genetic maps of kiwifruit and the identification of sex-specific markers. DNA Res.
837 2015;22: 367-375
- 838 35. Miller JS, Venable DL. Polyploidy and the evolution of gender dimorphism in plants.
839 Science. 2000;289: 2335-2338.
- 840 36. Zhou Q, Zhang J, Bachtrog D, An N, Huang Q, Jarvis ED, et al. Complex evolutionary
841 trajectories of sex chromosomes across bird taxa. Science. 2014;346: 1246338.

- 842 37. Dufresnes C, Borzée A, Horn A, Stöck M, Ostini M, Sermier R, et al. Sex-chromosome
843 homomorphy in palearctic tree frogs results from both turnovers and X-Y recombination.
844 Mol Biol Evol. 2015;32: 2328-2337.
- 845 38. Ahmed S, Cock JM, Pessia E, Luthringer R, Cormier A, Robuchon, et al. A haploid
846 system of sex determination in the brown alga *Ectocarpus* sp. Curr Biol. 2014; 24: 1945-
847 1957.
- 848 39. Bergero R, Qiu S, Forrest A, Borthwick H, Charlesworth D. Expansion of the pseudo-
849 autosomal region and ongoing recombination suppression in the *Silene latifolia* sex
850 chromosomes. Genetics. 2013;194: 673-686.
- 851 40. Ashman, TL, Spigler RB, Goldberg M, Govindarajulu R. *Fragaria*: a polyploid lineage
852 for understanding sex chromosome evolution. In: Navajas-Pérez R, editor. New insights
853 on plant sex chromosomes. Nova Science Publishers; 2012. pp. 67-90.
- 854 41. Liston A, Cronn R, Ashman TL. *Fragaria*: a genus with deep historical roots and ripe for
855 evolutionary and ecological insights. Am J Bot. 2014;101: 1686-1699.
- 856 42. Njuguna W, Liston A, Cronn R, Ashman T-L, Bassil N. Insights into phylogeny, sex
857 function and age of *Fragaria* based on whole chloroplast genome sequencing. Mol
858 Phylogenet Evol. 2013;66: 17–29.
- 859 43. Tennessen JA, Govindarajulu R, Liston A, Ashman TL. Targeted sequence capture
860 provides insight into genome structure and genetics of male sterility in a gynodioecious
861 diploid strawberry, *Fragaria vesca* ssp. *bracteata* (Rosaceae). G3 (Bethesda). 2013;3:
862 1341-1351.

- 863 44. Ashman TL, Tennessen JA, Dalton R, Govindarajulu R, Koski M, Liston A. Multilocus
864 sex determination revealed in two populations of gynodioecious wild strawberry,
865 *Fragaria vesca* subsp. *bracteata*. G3. 2015. doi: 10.1534/g3.115.023358
- 866 45. Tennessen JA, Govindarajulu R, Ashman TL, Liston A. Evolutionary origins and
867 dynamics of octoploid strawberry subgenomes revealed by dense target capture linkage
868 maps. *Genome Biol Evol.* 2014;6: 3295-3313.
- 869 46. Govindarajulu R, Parks M, Tennessen JA, Liston A, Ashman TL. Comparison of nuclear,
870 plastid, and mitochondrial phylogenies and the origin of wild octoploid strawberry
871 species. *Am J Bot.* 2015;102: 544-554.
- 872 47. Sargent, DJ, Yang Y, Šurbanovski N, Bianco L, Buti M, Velasco R, Giongo L, Davis
873 TM. HaploSNP affinities and linkage map positions illuminate subgenome composition
874 in the octoploid, cultivated strawberry (*Fragaria* × *ananassa*). *Plant Sci.* 2015;
875 doi:10.1016/j.plantsci.2015.07.004
- 876 48. Spigler RB, Lewers KS, Johnson AL, Ashman TL. Comparative mapping reveals
877 autosomal origin of sex chromosome in octoploid *Fragaria virginiana*. *J Hered.* 2010;
878 101 Suppl 1: S107-117.
- 879 49. Hancock JF and Bringham RS. Sexual dimorphism in the strawberry *Fragaria*
880 *chiloensis*. *Evolution* 1980;34: 762-768.
- 881 50. Ashman T-L. The limits on sexual dimorphism in vegetative traits in a gynodioecious
882 plant. *Am Nat.* 2005;166 Suppl 4: S5-16.

- 883 51. Darwish O, Shahan R, Liu Z, Slovin JP, Alkharouf NW. Re-annotation of the woodland
884 strawberry (*Fragaria vesca*) genome. BMC Genomics. 2015;16: 29.
- 885 52. Hirakawa H, Shirasawa K, Kosugi S, Tashiro K, Nakayama S, Yamada M. Dissection of
886 the octoploid strawberry genome by deep sequencing of the genomes of *Fragaria*
887 species. DNA Res. 2014; 21: 169-181.
- 888 53. Charlesworth B. The evolution of chromosomal sex determination and dosage
889 compensation. Curr Biol. 1996;6: 149-162.
- 890 54. Bomblies K, Higgins JD, Yant L. Meiosis evolves: adaptation to external and internal
891 environments. New Phytol. 2015;208: 306-323.
- 892 55. Shilo S, Melamed-Bessudo C, Dorone Y, Barkai N, Levy AA. DNA crossover motifs
893 associated with epigenetic modifications delineate open chromatin regions in
894 Arabidopsis. Plant Cell. 2015;27: 2427-2436.
- 895 56. Spigler RB, Ashman T-L. Sex ratio and subdioecy in *Fragaria virginiana*: the roles of
896 plasticity and gene flow examined. New Phytol. 2011;190: 1058-1068.
- 897 57. Govindarajulu R, Liston A, Ashman T-L. Sex-determining chromosomes and sexual
898 dimorphism: insights from genetic mapping of sex expression in a natural hybrid
899 *Fragaria* × *ananassa* subsp. *cuneifolia*. Heredity (Edinb). 2013;110: 430-438.
- 900 58. Li J, Koski MH, Ashman T-L. Functional characterization of gynodioecy in *Fragaria*
901 *vesca* ssp. *bracteata* (Rosaceae). Ann. Bot. (Lond.) 2012; 109: 545–552.

- 902 59. Akagi T, Henry IM, Tao R, Comai L. A Y-chromosome-encoded small RNA acts as a
903 sex determinant in persimmons. *Science*. 2014;346: 646-650.
- 904 60. Pucholt P, Rönnerberg-Wästljung AC, Berlin S. Single locus sex determination and female
905 heterogamety in the basket willow (*Salix viminalis* L.). *Heredity (Edinb)*. 2015;114: 575-
906 583.
- 907 61. Ahmadi H, Bringham RS. Genetics of sex expression in *Fragaria* species. *American*
908 *Journal of Botany* 1991;78: 504-514.
- 909 62. Charlesworth D. Allocation to male and female function in hermaphrodites, in sexually
910 polymorphic populations. *J Theor Biol*. 1989;139: 327-342.
- 911 63. Pennell TM, Morrow EH. Two sexes, one genome: the evolutionary dynamics of
912 intralocus sexual conflict. *Ecol Evol*. 2013; 3: 1819–1834.
- 913 64. Chen L, Liu Y-G. Male sterility and fertility restoration in crops. *Annu Rev Plant Biol*.
914 2014;65: 579-606.
- 915 65. Besouw MT, Kremer JA, Janssen MC, Levchenko EN. Fertility status in male cystinosis
916 patients treated with cysteamine. *Fertil Steril*. 2010;93: 1880-1883.
- 917 66. Field DL, Pickup M, Barrett SC. Comparative analyses of sex-ratio variation in dioecious
918 flowering plants. *Evolution*. 2013;67: 661-672.
- 919 67. Muller HJ. The relation of recombination to mutational advance. *Mutat Res*. 1964;106: 2-
920 9.

- 921 68. Ma H, Moore PH, Liu Z, Kim MS, Yu Q, Fitch MM, et al. High-density linkage mapping
922 revealed suppression of recombination at the sex determination locus in papaya.
923 Genetics. 2004;166: 419-436.
- 924 69. van Os H, Andrzejewski S, Bakker E, Barrena I, Bryan GJ, Caromel B, et al.
925 Construction of a 10,000-marker ultradense genetic recombination map of potato:
926 providing a framework for accelerated gene isolation and a genomewide physical map.
927 Genetics. 2006;173: 1075-1087.
- 928 70. Miao H, Zhang S, Wang X, Zhang Z, Li M, Mu S, et al. A linkage map of cultivated
929 cucumber (*Cucumis sativus* L.) with 248 microsatellite marker loci and seven genes for
930 horticulturally important traits. Euphytica 2011;182: 167-176.
- 931 71. Papadopulos AS, Chester M, Ridout K, Filatov DA. Rapid Y degeneration and dosage
932 compensation in plant sex chromosomes. Proc Natl Acad Sci U S A. 2015;112:13021-
933 13026.
- 934 72. Nachman MW. Variation in recombination rate across the genome: evidence and
935 implications. Curr Opin Genet Dev. 2002;12: 657-663.
- 936 73. Natri HM, Shikano T, Merilä J. Progressive recombination suppression and
937 differentiation in recently evolved neo-sex chromosomes. Mol Biol Evol. 2013;30: 1131-
938 1144.
- 939 74. Blaser O, Neuenschwander S, Perrin N. Sex-chromosome turnovers: the hot-potato
940 model. Am Nat. 2014;183: 140-146.

- 941 75. van Doorn GS, Kirkpatrick M. Transitions between male and female heterogamety
942 caused by sex-antagonistic selection. *Genetics*. 2010;186: 629-645.
- 943 76. R Core Team. R: A language and environment for statistical computing. R Foundation
944 for Statistical Computing, Vienna, Austria. 2013. <http://www.R-project.org/>.
- 945 77. Margarido GR, Souza AP, Garcia AA. OneMap: software for genetic mapping in
946 outcrossing species. *Hereditas*. 2007;144: 78-79.
- 947 78. Broman, KW, Wu H, Sen S, Churchill GA. R/qtl: QTL mapping in experimental crosses.
948 *Bioinformatics* 2003;19: 889–890.
- 949 79. Cronn R, Knaus BJ, Liston A, Maughan PJ, Parks M, Syring JV, et al. Targeted
950 enrichment strategies for next-generation plant biology. *Am J Bot*. 2012;99: 291-311.
- 951 80. Byers RL, Harker DB, Yourstone SM, Maughan PJ, Udall JA. Development and
952 mapping of SNP assays in allotetraploid cotton. *Theor Appl Genet*. 2012;124: 1201-1214.
- 953 81. Uribe-Convers S, Settles ML, Tank DC. A targeted subgenomic approach for
954 phylogenomics based on microfluidic PCR and high throughput sequencing. 2015. doi:
955 <http://dx.doi.org/10.1101/021246>
- 956 82. Bolger AM, Lohse M, Usadel B. Trimmomatic: A flexible trimmer for Illumina
957 Sequence Data. *Bioinformatics*. 2014;30: 2114-2120.
- 958 83. Li H, Durbin R. Fast and accurate short read alignment with Burrows-Wheeler transform.
959 *Bioinformatics*. 2009;25: 1754-1760.

960 84. Li H, Handsaker B, Wysoker A, Fennell T, Ruan J, Homer N, et al. The Sequence
961 alignment/map (SAM) format and SAMtools. *Bioinformatics*. 2009;25: 2078–2079.

962 85. Diedenhofen B, Musch J. cocor: A Comprehensive Solution for the Statistical
963 Comparison of Correlations. *PLoS ONE*. 2015;10: e0121945

964 86. Shulaev V, Sargent DJ, Crowhurst RN, Mockler TC, Folkerts O, Delcher AL, et al. The
965 genome of woodland strawberry (*Fragaria vesca*). *Nat Genet*. 2011;43: 109-116.

966

967 **Supporting information captions**

968 **S1 Table.** Phenotypes and genotypes for all HM×SAL offspring.

969 **S2 Table.** Phenotypes and genotypes of EUR and PTR offspring.

970 **S3 Table.** IDs and collection localities of plants unrelated to the parents of the crosses.

971 **S4 Table.** Positions of all markers in target capture linkage maps.

972 **S5 Table.** List of 70 genes in the 280kb window on Fvb reference chromosome 6 matching the

973 *F. chiloensis* SDR

974 **S6 Table.** Recombination rates for all linkage groups.

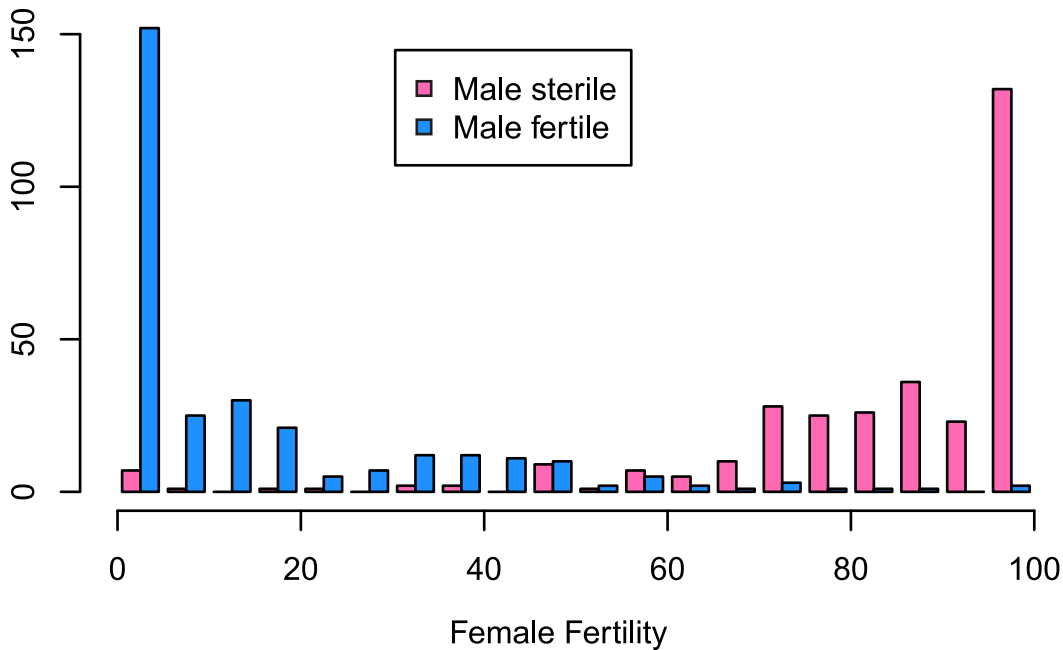
975 **S7 Table.** Primers for amplicon sequencing

976 **S8 Table.** PCR conditions for all amplicons.

977 **Fig S1. Haplotypes in the SDR vicinity.** We resolved twelve haplotypes, two from each of the
978 parents of three crosses (diagonally shaded bars). For the additional unrelated plants, we did not
979 phase haplotypes but instead show all SNPs present in each diploid genotype (solid bars). SNPs
980 that mapped to VI-Av-m in at least one cross were observed from amplicons (indicated with
981 X's), and are plotted with an x-axis position corresponding to physical position on reference
982 genome chromosome Fvb6. Within a haplotype, SNPs are staggered vertically if more than one
983 occurred in the same amplicon. SNPs are categorized based on whether they are ever observed in
984 coupling with sex (circles) or not (squares). The universal marker showing a correlation with sex
985 across most plants is shown as a solid circle. A high density of SNPs in coupling with sex occurs
986 in the SDR, especially in the “high W divergence” region from 37.565-37.708Mb.

987

Count of Individuals



LOD to Male Function

